Defence Research and Development Canada | Recherche et développement pour la défense Canada

CAN UNCLASSIFIED

DRDC | RDDC
technologysciencetechnologie

Development of Advanced Imaging Algorithms and Representations for Compton Gamma-Ray Cameras

Christian Van Ouellet
Zernam

Prepared by:
Zernam
1701 Woodward Dr, Suite 100
Ottawa, ON K2C 0R4 Canada

PSPC Contract Number: W7714-4501560211
Technical Authority: Pierre-Luc Drouin
DRDC – Ottawa Research Centre
Contractor's date of publication: October 2017

Defence Research and Development Canada
Contract Report
DRDC-RDDC-2018-C074
April 2018

Canada

IMPORTANT INFORMATIVE STATEMENTS

This document was reviewed for Controlled Goods by Defence Research and Development Canada (DRDC) using the Schedule to the *Defence Production Act*.

Abstract

DRDC has produced a toolkit of imaging algorithms which are suitable for any segmented Compton gamma ray imager. The algorithms incorporate a completely novel, three dimensional tessellated geodesic mesh representation for the data. The geodesic representation is fully recursive to include arbitrary resolution and furthermore resolves projection artifacts of other common imaging systems. As part of the partnership between DRDC, NRC and Radiation Solutions Inc., a fully functional rugged Compton imager has been successfully manufactured for the Canadian Armed Forces. DRDC imaging algorithms have been integrated into the imager software and provide reliable, fast options for radioactive threat detection.

Résumé

RDDC a produit une boîte à outils d'algorithmes d'imagerie qui conviennent à tout imageur à rayons gamma Compton segmenté. Les algorithmes incorporent une représentation en treillis géodésique tridimensionnelle complètement nouvelle pour les données. La reprèsentation géodésique est entièrement récursive pour inclure une résolution arbitraire et résout en outre les artefacts de projection d'autres systèmes d'imagerie courants. Dans le cadre du partenariat entre RDDC, le CNRC et Radiation Solutions Inc., un imageur Compton robuste et entièrement fonctionnel a été fabriqué avec succès pour les Forces Armées Canadiennes. Les algorithmes d'imagerie de RDDC ont été intégrés dans le logiciel de l'imageur et offrent des options fiables et rapides pour la détection des menaces radioactives.

This page intentionally left blank.

Table of contents

Abstract i

Résumé i

Table of contents iii

List of figures v

1 Introduction to Compton Imaging 1

2 Imaging Algorithms 3

2.1 Detailed Code Structure and User's Manual 3

2.2 Mercator View 5

3 Using the Algorithms 7

3.1 Back Projection 8

3.2 LMMLEM: List Mode Maximum Likelihood Expectation Minimization 8

3.3 SOE: Stochastic Origin Ensembles method 8

4 Implementation of Tessellated Geodesic Mesh 9

4.1 Observer View 10

4.2 Multi-source Tests 12

4.3 Eye rotation Tests 13

4.4 Real World Imaging 14

5 Sample High Statistics Monte Carlo Visualizations of a Point Source . . . 16

5.1 Back Projection 16

5.2 LMMLEM 17

5.3 SOE 18

6 Applications and Extensions of Imaging Code 19
6.1 Jiffy imaging 19
6.2 Large and small “L” imaging 21
7 Finalized Instrument at NRC 24
7.1 Final physical device 24
7.2 Integration into NRC code framework 27
7.3 Hardware limitations 28
7.4 NRC lab testing 28
7.5 Adjustments for optical lens image distortion 29
7.6 Field testing of the completed system 33
7.7 Potential improvements 35
8 Summary and Conclusions 36
References 37

List of figures

Figure 1: Geant4 visualization of the detector geometry 2

Figure 2: Sample Doxygen inheritance and collaboration diagram for the BackProjection class. 4

Figure 3: The Mercator projection (a) this naive projection has the underlying problems of a cylindrical representation (b) the globe, note the apparent size of Russia relative to Africa (c) the African continent is in area much larger than Russia. 6

Figure 4: A common frequency division tessellation of the sphere. 9

Figure 5: Our specific tessellation scheme. 10

Figure 6: The ultimate goal of the Observer View is to provide a seamless window through which to view the world of gamma-rays super-imposed upon the viewer's window. The framework for something as sophisticated and user-friendly as this pictured cell-phone view now exists. Future developments could marry the gyroscope tracking technology of common cell phones to allow for a mobile viewing platform. As of now, with the end of the current research project, the aim was to build the functionality in but only for a fixed screen location. 11

Figure 7: Imaging of multiple sources - (a) Back Projection (b) SOE (c) LMMLEM. Leftmost source is half the intensity of the centre-most source. Furthest source is the same intensity as the centre-most, its reduced visual impact is entirely due to being off-centre with the corresponding lowered detector sensitivity. . . 12

Figure 8: The observer magic window is free to move within the geodesic tessellation - in (a) the observer is staring straight at the same three sources as the previous section, in (b) the observer tilts his head 45 degree to the right and the visualization moves as anticipated left, in (c) the observer tilts his head 45 degrees up from the centred position and the sources likewise are displaced as anticipated down. 13

Figure 9: Raw image of a colorful, difficult to image bridge. Prague, capital of the once Holy Roman Empire. 14

Figure 10: Multi-source imaging back projection translucent overlay. Second source is difficult to disambiguate. 15

Figure 11: Reduced threshold and higher contrast provides much better visual source detection. 15

Figure 12: Back projection, 200 000 Compton cones ^{137}Cs (a) Mercator square grid (b) Mercator geodesic triangles projection (c) Observer view. The tessellation level is set to 8 in all figures. . . . 16

Figure 13: LMMLEM, 200 000 Compton cones ^{137}Cs (a) Mercator square grid (b) Mercator geodesic triangles projection (c) Observer view. The tessellation level is set to 8 in all figures and the Observer window is a field of view of 112 degrees horizontally and 90 degrees vertical. 17

Figure 14: SOE, 200 000 Compton cones ^{137}Cs (a) Mercator square grid (b) Mercator geodesic triangles projection (c) Observer view. The tessellation level is set to 8 in all figures and the Observer window is a field of view of 112 degrees horizontally and 90 degrees vertical. 18

Figure 15: Real data from Jiffy imager for ^{137}Cs (a) Back Projection (b) SOE (c) LMMLEM. The LMMLEM algorithm appears to be the winner by eye. 19

Figure 16: Real data from Jiffy imager for ^{22}Na (a) Back Projection (b) SOE (c) LMMLEM. With these lower counts and this different source, factoring all the variables it appears that SOE better resolves the source. These results are a bit surprising as naively SOE should function better with larger sample size, however the main purpose of this research is to empirically test rather than speculate. The immediate conclusion from visual inspection drawn from even these limited tests: for the end user both imaging algorithms should be made available and allow their judgment in the field to prevail. 20

Figure 17: The UAV is flown in a raster pattern represented by the large black dots over a large distributed “L” shaped source, seen in black outline. The Compton camera takes an image for 1 second at the location of the dots. Each resulting Mercator projection is stitched together to form a composite view, revealing the shape of the underlying activity. 22

Figure 18: Similar to Fig.17 but with a much smaller "L" source, merely 7 x 6 m. This size of distributed source is specifically at the limit of the spatial sampling and realistically once detected the individual snapshots directly above the source would be investigated and the collating multiple views from multiple angles would be foregone. . 22

Figure 19: The Observer View snapshot of the single position directly above the small L. The distributed source legs are clearly distinguishable. 23

Figure 20: The finalized imager on a cart, its camera clearly visible in front. In the background on a table, the JIFFY. 24

Figure 21: Detector internals (front side). The 3x3 absorber and scatter array were mounted on rails, to preserve the option to change the focal length of the array. The mainboard sat below with its custom chipset. The SiPM were connected via the mass of cabling to channel readout daughter cards (8 in total). The camera was solidly affixed along the central symmetry axis of the array. . . . 25

Figure 22: Detector internals (rear side). The Advantech computer (Compton 5) communicated to the mainboard through USB. Compton 5 was in turn controlled via laptop through proprietary RAD-ASSIST software, through ethernet. A switch managed ethernet and power to the internals. 25

Figure 23: The default projection assumed within "Observer View". This is a straightforward projection of a unit geodesic sphere onto the user's screen, the only knowledge required to perform this is the angle at which the observer sees through the magic window, θ, relative to the imager's central axis. 29

Figure 24: In the real world application the image is captured using a camera and a lens. The lens introduces significant distortion in the optical image, however the physical angles derived from the absorber and scatter hits do not have such distortion. The problem is then to relate the apparent angle at which objects are seen in the camera projected image, θ to their true angle as seen by the imager, θ_{True}. For the specific lens used it was empirically determined a simple tangent formulation was sufficient. 30

Figure 25: The optical image was captured in 1080p format, 1920x1080 pixels. The camera was first carefully and properly aligned along the imager's central axis. An object seen at pixel X away from the central pixel corresponded to a real world angle of θ, an object seen at pixel 2X away from the central pixel corresponded to a real world angle of twice θ, and so on. Equally spaced angles were thus distorted by the lens into an equally spaced line. 31

Figure 26: Camera imaging of the NRC test hall. The large red dot represents the true source position (top). The yellow and black striped tape on the ground is in fact a straight line in the real world, it appears warped into a curve as a result of the lens. With the angular correction applied (bottom) back projection Observer View overlays properly with the off-axis source in the display. . . 32

Figure 27: End-user imaging of a ^{137}Cs source at NRC part 1. This image is a screen shot capture of the RAD-ASSIST program which runs on a laptop connected to the Compton imager. On the left is a continuously updating "waterfall" plot of the energy spectrum: every 1 second the energy spectrum is read out and continuously incrementing from below in a coloured band. This allows for the user to potentially identify changes in the detected radiation based on energy alone. In this instance the source has remained in its fixed location and the spectrum has been accumulating for 10 minutes. The sum energy spectrum, the projection of the waterfall plot is displayed in the bottom left corner and the Cs line is clearly visible. The user has yet to engage imaging and merely knows from the energy spectrum and alarms that something is present but is unaware of the source location. 33

Figure 28: End-user imaging of a ^{137}Cs source at NRC part 2. The user has selected a band in the waterfall plot corresponding to the energy peak of his interest. The imaging algorithm is thus activated and in less than 1 second the geodesic LMMLEM is overlayed upon the camera output identifying the most probably location of the radioactivity successfully. 34

1 Introduction to Compton Imaging

The detection, localization and identification of gamma-emitting radioactive sources is an essential element of emergency response for security and military within the context of a radiation threat. A Compton gamma imager provides these three features in a single device and its development was funded by the Department of National Defence (DND) in collaboration with the National Research Council (NRC) [1] and Natural Resources Canada (NRCan) [2].

In its simplest design a Compton imager consists of two layers of gamma-ray detectors, a thin scattering layer and a thick absorber layer, with each layer segmented in an x-y plane.

Many types of gamma interaction are possible within the detector, but those of particular interest for imaging purposes must satisfy a specific constraint: The gamma must scatter only once in the scatter layer and be completely absorbed in the absorber layer.

Such events while rare allow for the Compton angle θ_C between the incident direction of the gamma ray and the scattered ray to be calculated from the energy deposits. Thus the direction of the incident ray can be estimated up to a cone (Fig.1) and the further segmentation of the array allows for a pixelated refinement of the direction of the cone axis [3].

$$\cos(\theta_C) = 1 + m_e c^2 \left[\frac{1}{E_{total}} - \frac{1}{E_{absorber}} \right] \tag{1}$$

With the collection of multiple such events the overlap of these "Compton cones" points towards the location of the source (Fig. 1). NRC has coordinated assembly of various prototype imagers and the first field ready imager for the Canadian forces, the SCoTSS (Silicon Compton Telescope for Safety and Security) [4]. The crystals selected for the imaging modules are composed of thallium-doped cesium iodide (CsI(Tl)) and the scintillation light from the crystals is collected using silicon photomultipliers (SiPM). SiPMs are solid state avalanche photodiode arrays with similar functional capabilities to traditional photomultiplier tubes (PMT) except that they are much less fragile. The combination of CsI and SiPMs provides a rugged, compact, room temperature, low power consumption alternative to current off-the-shelf Compton imager models which often rely on cryogenically cooled Germanium crystals and delicate glass and vacuum PMTs.

Previous reports [5] [6] investigated the GEANT model used to describe the imager's properties as well as potential improvements over energy spectrum source detection using the likelihood ratio method and spatial data. Several imaging algorithms were

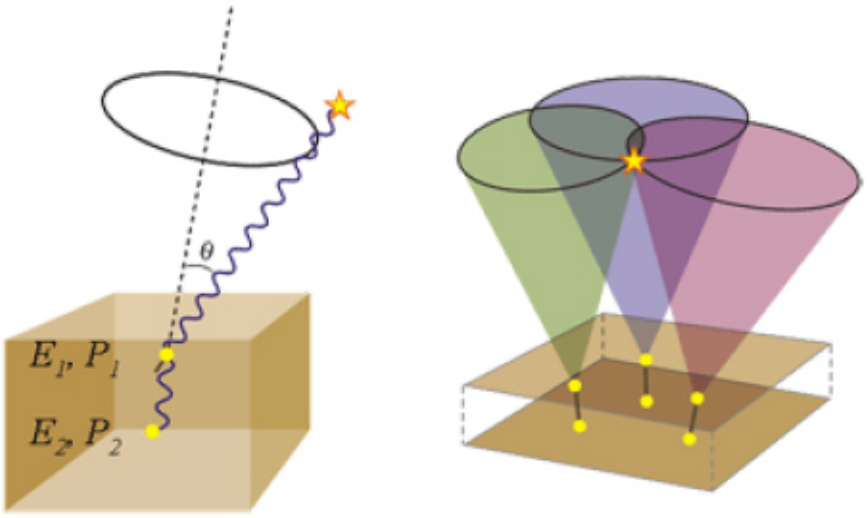

Figure 1: *Schematic illustration of a Compton camera. Two layers of gamma-ray detectors and several overlaps of Compton cones can provide the location of initial gamma-ray source.*

also developed along with some limited testing on simulated sources. The research also revealed a problem of all Compton imagers to date: the projection method by which Compton ring data is presented to users distorts the importance of cones along high polar angles. Work began on a geometrically proper physical projection onto a tessellated geodesic field of view. The present report details the culmination of the imaging algorithm work, with the final form of imaging algorithm codes and their application to real data and detailed simulations. The geodesic "true projection" view is fully implemented and shown to be intuitive and great step forward in the end user's ability to locate sources of radioactivity.

2 Imaging Algorithms

Three specific algorithms were developed for imaging, back projection, LMMLEM and SOE, each with their own particular benefits as will be detailed in this section. All algorithms were designed for general imaging, in other words the specific construction of the Compton imager does not impact their functionality, the algorithms are completely general and can be ported from one design to another, as will be seen in the later section on applications. Furthermore the algorithms are insensitive to the specifics of the source they are imaging, they function equally as well with a point source, multiple point sources or distributed sources.

2.1 Detailed Code Structure and User's Manual

The analysis pipeline detailed in [6] was streamlined and extensively optimized for speed. ROOT is a free and GNU public license physics analysis software platform extensively used in nuclear and particle physics analysis [7]. Because the end product is to be a commercially available instrument those portions of the code that previously used ROOT classes are now native C++. The present codes only bear superficial resemblance to iterations discussed in previous reports, current codes are production level quality, heavily commented and come with detailed Doxygen documentation [8]. A sample of the diagrams that Doxygen produces for ease of understanding code structure can be seen in Fig.2.

Imaging is the super-class and executable. Data from the Compton imager in the form of the Compton angle, and the vector components of the principle axis of the cone are fed into the ImagingInputData class. The data need not be processed through CIAnalysis, so long as the particular angular coordinates used to interpret the cone vectors are used, but if the data is processed through CIAnalysis the quality of the events is further checked looking at associated hitflags. Only golden events (`hitflag == 35`) are used in imaging.
ImagingInputData references the user defined ImagingInputCoordinateSystem. This input coordinate system can be either the "traditional" Mercator projection scheme or the advanced GeodesicTriangles system. The imaging input data is then processed and stored into data type ring structures, either square-grid rings or geodesic triangles rings. Note some English language confusion is possible here: these are programming ring structures that hold Compton cone data, which when projected onto the input coordinate system appear as "rings". These ring structures are highly optimized with their own internal binning schemes, they store linked lists of bins that the Compton cone projection intersects. For a given Compton cone, each bin within the linked list stores the arc length fraction of the Compton cone projection. The sum of all the arc length fractions from all the Compton cone projection bins is defined as one, and thus

each bin stores the probability of the photon originating from that particular bin. It is this fraction of arc length calculation that is the most computationally intensive operation of the code, hence requiring the special coding, looping over all bins within an ImagingInputCoordinateSytem would have many empty bins and would scale terribly with higher resolutions.
Once the arc lengths are processed into ring structures ImagingInputData retains these in memory. Multiple algorithms can now access the ImagingInputData without re-processing, so long as the InputCoordinateSystem is not modified. In this way the end user can flip between different imaging algorithms quickly, only the specific imaging algorithm is run rather than reprocess the input data repeatedly.

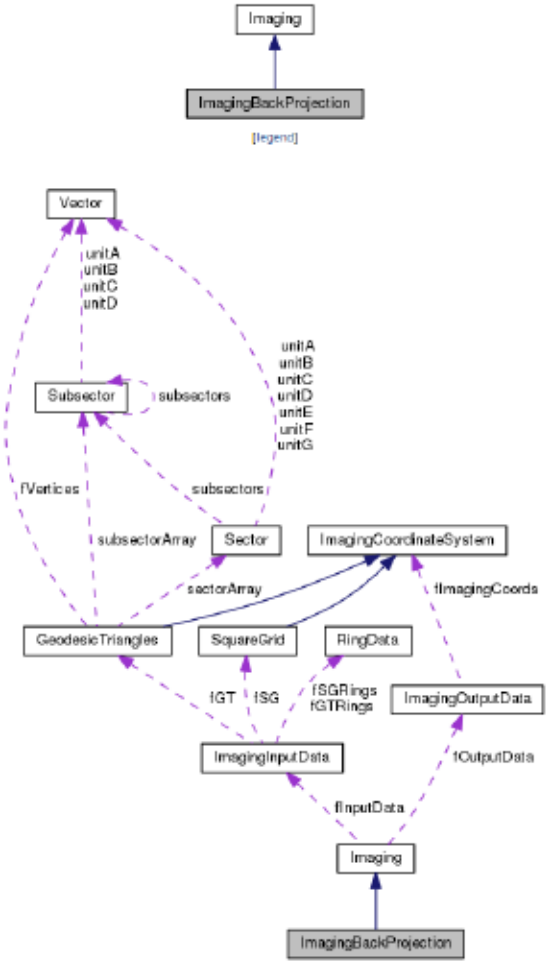

Figure 2: *Sample Doxygen inheritance and collaboration diagram for the BackProjection class.*

The ImagingInputData is then passed to the specific daughter class algorithms of Imaging, Back Projection, LMMLEM or SOE and these produce ImagingOutput-

Data. The user must have selected an ImagingOutputCoordinateSystem, this output coordinate system for the case of Back Projection and LMMLEM must be identical. For SOE the output coordinate system can be lower resolution that the input system, this takes advantage of a special property of the SOE algorithm. The ImagingOutputData is still abstract data, an array with the list of bins for the output coordinate system and the associated value the imaging algorithms have assigned them, at this stage the data needs to be translated into something the end user can interpret.
The ImagingRepresentation is what the end user actually sees on his screen. Imaging representations are of two types, the first is a widely used but flawed visual perspective angular binning - the Mercator representation, the second is a novel development of this specific research - the Observer View representation. Observer View will be discussed in its own section, the following describes the Mercator representation.

2.2 Mercator View

When nautical cartographers first began mapping the world they devised various systems for projecting the spherical globe onto a horizontal plane and chief amongst these is the Mercator projection from Flemish geographer and cartographer Gerardus Mercator in 1569. Mathematically it is a conformal cylindrical projection that preserves angles, it is for this reason that the globe represented in this view is functional for navigation. but unimportant for navigation, distorts areas. The surface area of Russia which lies close to the north pole is for instance grossly exaggerated relative to the continent of Africa. The problem for representing Compton imaging in an intelligible fashion to the end user is the self same as the ancient cartographers, unravelling the sphere onto a 2-D computer screen so that the source of radioactivity can be located. The Compton imaging community has accepted for a variety of reasons (primarily convenience) to use a Mercator projection in imaging where the observer sits at the origin, the location of the detector, along with a modified form of true polar angles. The azimuthal angle is defined along the plane of the ground with the zero axis pointing directly along the principle axis of the detector array and the zenith angle is importantly not the true polar zenith either, but with zero also along the principle axis. This coordinate system is useful in the regard that it is somewhat intuitive for an end-user, positive azimuthal is turning your head to your right, positive zenith is turning your head up and vice versa for negative angles to the left and down. It is also not an entirely unreasonable representation since most of the sensitivity of a planar array such as the current Compton imager is focused along the axis, cones from higher angles are severely suppressed. So long as one restricts the imaging field of view to a narrow range of angles at the equator Mercator projections are approximately correct. Nonetheless it remains a fundamentally flawed imaging representation, polar bins are vastly distorted in importance, however as a community “standard" view it is useful to include in this code alongside the much more advanced Observer View.

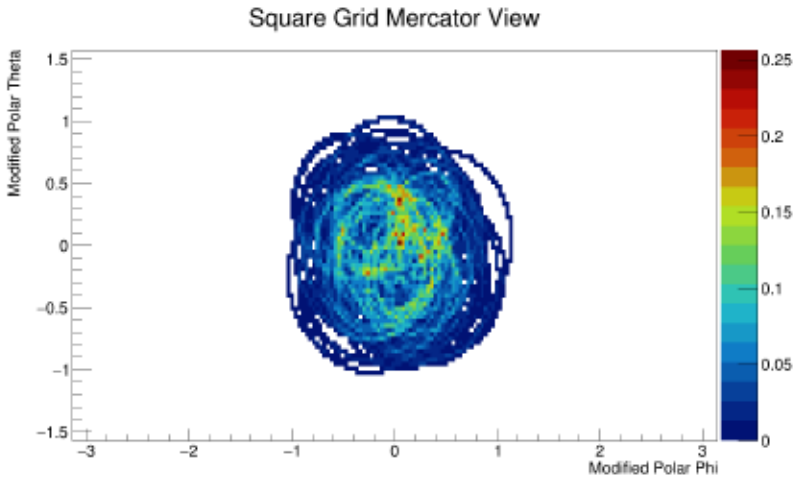

(a)

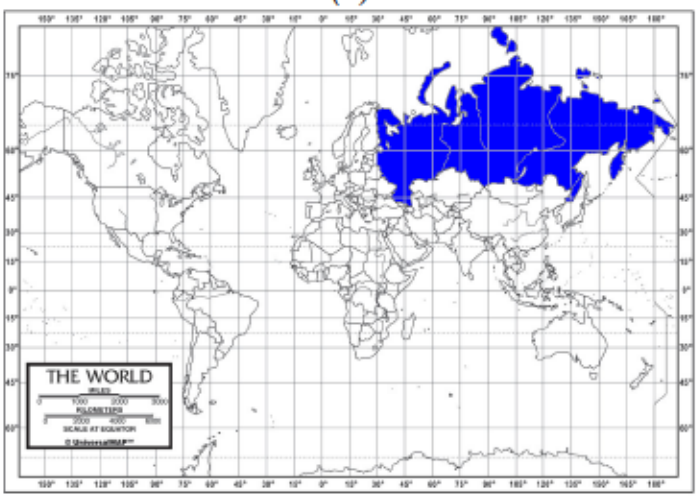

(b)

(c)

Figure 3: *The Mercator projection (a) this naive projection has the underlying problems of a cylindrical representation (b) the globe, note the apparent size of Russia relative to Africa (c) the African continent is in area much larger than Russia.*

3 Using the Algorithms

The algorithms are designed to run on processed 2-hit Compton cone data. For historical reasons detailed within the code comments this data consists of a list with the following designations: Compton angle in radians ("radius"), hitflags ("37 = golden"), angle between the scatter hit and absorber hit and the z-axis ("cx", "cy"). "Imaging" is the executable and always accepts the following flags:

```
> ./Imaging --in inFile
                [--BackProjection --LMMLEM --SOE] outFile
                [--Num number]

                [--inGT] [--outGT] [--GTlevel gtl]
                [--ObserverView]
                [--PhiEye phi] [--ThetaEye theta]

                [--inSG] [--outSG] [--SGnbins sn]
                [--MercatorView]
```

- gtl is an integer, number of recursive geodesic triangle levels (default: 8)
- sn is an integer, number of bins in the square grid
- number is an integer, total number of events to process, useful to not process entirety of a large file.
- phi is a float, observer's eye direction along the horizontal in radians
- theta is a float, observer's eye direction along the vertical in radians

inGT and outGT must be selected for ObserverView output.
MercatorView works with either geodesic triangles GT or square grid SG.

3.1 Back Projection

The back projection algorithm is precisely the simplest and essential form of imaging using a Compton camera [9]. An additional form of back projection, dubbed two cone back projection was investigated in the past but deemed superfluous relative to the much better filtering of LMMLEM and SOE for comparable speed.

3.2 LMMLEM: List Mode Maximum Likelihood Expectation Minimization

LMMLEM estimates the source distribution from observed events using a response matrix - it builds an image through a defined number of iterations, the value of the likelihood function at each iteration increases the estimate [10]. Another interesting aspect of the type of LMMLEM implemented is that it has a natural extension that accounts for differing detector sensitivity. In essence the angular detector efficiency can be readily factored into the response matrix [11]. The framework for this was built, but not implemented at the time of this report's writing. Additional LMMLEM specific flags are as follows:

```
> ./Imaging --in inFile --LMMLEM outFile
                [--MLEMNIters iter] [--SensitivityMap]
```

where iter is an integer hard iteration cut.

3.3 SOE: Stochastic Origin Ensembles method

SOE is a Markov-Chain Monte Carlo approach to image reconstruction [12] [13]. The Metropolis-Hastings algorithm [14] is used as a method to judge between samples. A detailed DRDC report exists on the implementation of this algorithm [15].

```
> ./Imaging --in inFile --SOE outFile
                [--outGTlevel oGT] [--outSGnbins oSG]
```

SOE is the only algorithm where the input and output coordinate system need not match in number of bins, oGT and oSG need to be corresponding integers. This can be useful in the case of sparse data, SOE can struggle if input data is binned too fine.

4 Implementation of Tessellated Geodesic Mesh

Tessellating a sphere is a long understood mathematical problem with no singular best solution. The goal of preserving areas in a projection of the sphere however cannot easily be met by squares. More often triangles are used as the base shape. The fifth and final platonic solid, constructed of congruent regular polygonal faces is the icosohedron, built from 20 triangles. A common method of tessellation is to further sub-divide the facets of the icosohedron into equilateral triangles and then project their vertices onto the sphere as seen in Fig.4. This form of tessellation makes comparison between 2 different frequency divisions difficult as the bins shift relative to one another rather than merely enhance resolution. We decided to go with equal area subtriangles and to always subdivide along the longest side.
In our particular tessellation these 20 facets form the base and are called sectors. Each sector is subdivided into 6 equal area triangles following the triangle centroid, these 6 triangles correspond to first layer of subsectors as seen in Fig.5. For every further frequency each triangle is then divided into 2 equal area triangles forming the next layer of subsectors. The code as constructed is recursive, an arbitrary frequency can be generated and so correspondingly an arbitrary resolution requested. For reference as user input: layer zero corresponds to 20, layer 1 to 120, layer 2 to 240 and so forth.

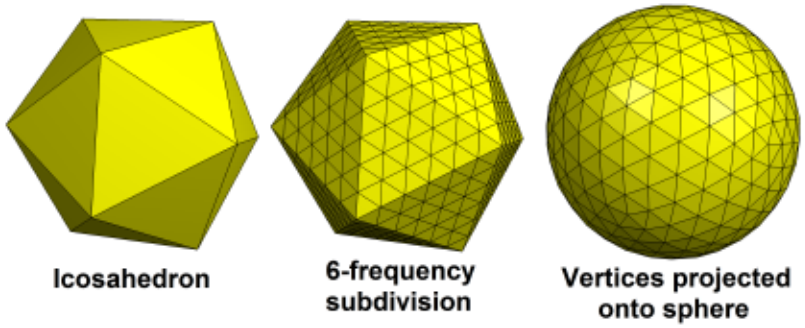

Figure 4: *A common frequency division tessellation of the sphere.*

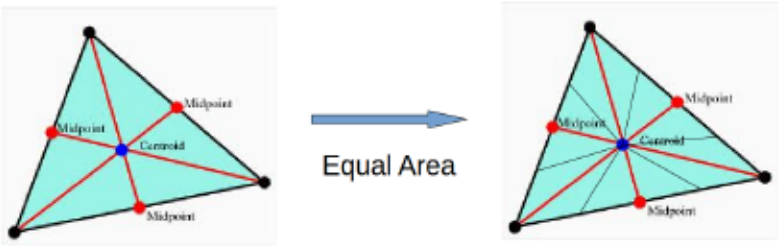

Figure 5: *Our specific tessellation scheme.*

4.1 Observer View

The Observer View is to provide the user with a completely intuitive window through which to visually identify radioactivity with geometrically perfect projection. In other words: a "magic" window through which one can see the world in gamma rays as though you were the detector. This is best understood through a picture as in Fig.6. The rectangular window dimensions can be adjusted to any size and position that will fit within the unit sphere, allowing for instance a wide range of view or as narrow a band as desired, in essence the position of the magic window relative to the observer. All Observer View figures within this document correspond to an observer's eye at the centre of a unit sphere, with a rectangular window 0.1 units in front of him, and window aspect ratio of 0.3 and 0.2 on a side. This corresponds to a field of view of 112 degrees horizontally and 90 vertically.

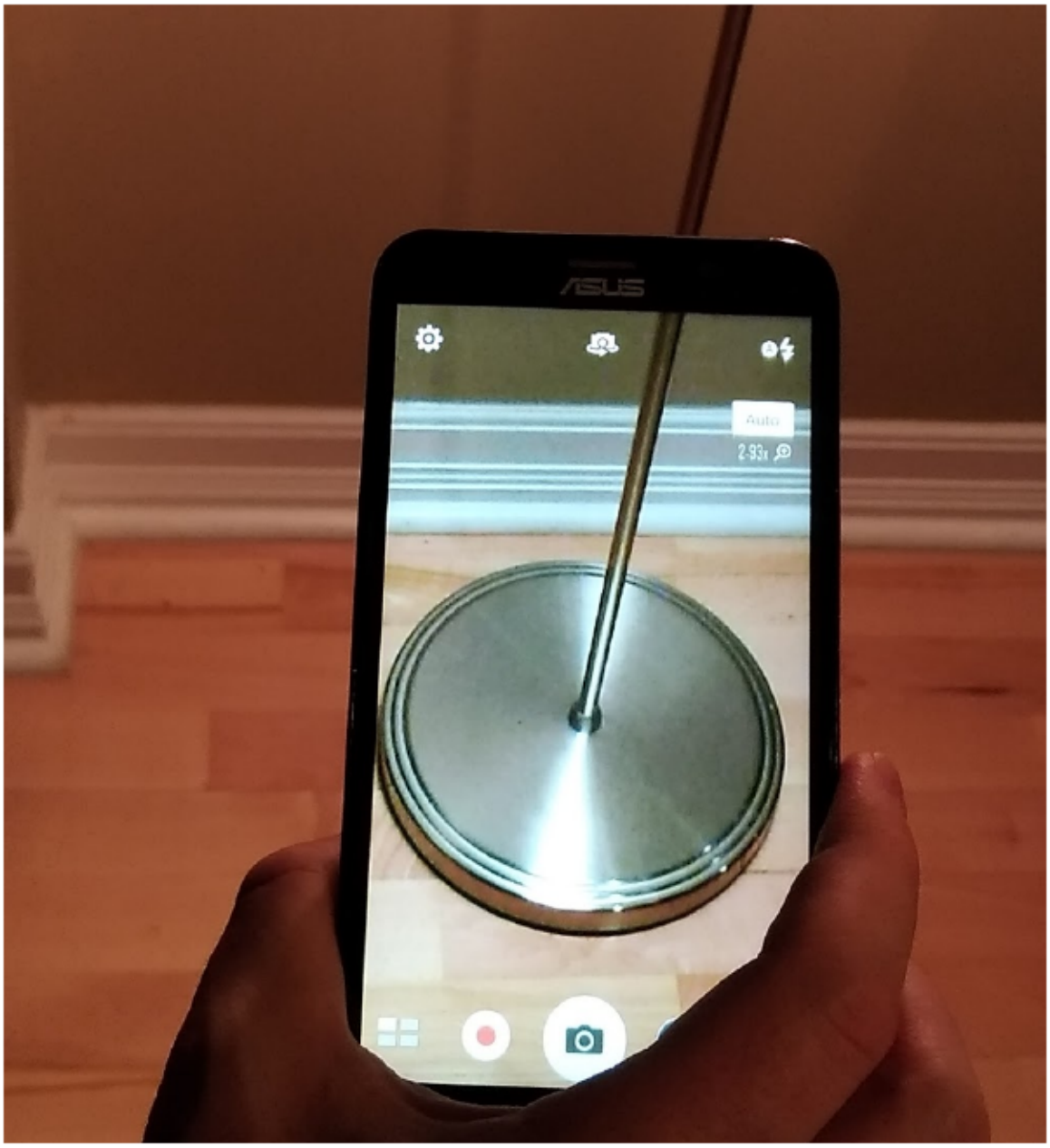

Figure 6: *The ultimate goal of the Observer View is to provide a seamless window through which to view the world of gamma-rays super-imposed upon the viewer's window. The framework for something as sophisticated and user-friendly as this pictured cell-phone view now exists. Future developments could marry the gyroscope tracking technology of common cell phones to allow for a mobile viewing platform. As of now, with the end of the current research project, the aim was to build the functionality in but only for a fixed screen location.*

4.2 Multi-source Tests

Several simulations of multiple sources were performed to test for their visual impact and provide reassurance the algorithms could not be confused by multiple strong sources. The results can be seen in Fig.7 and it is clear that the algorithms perform well irrespective of the number of sources. Statistics are 50 000 cones total of ^{137}Cs, all at 10 m from the imager.

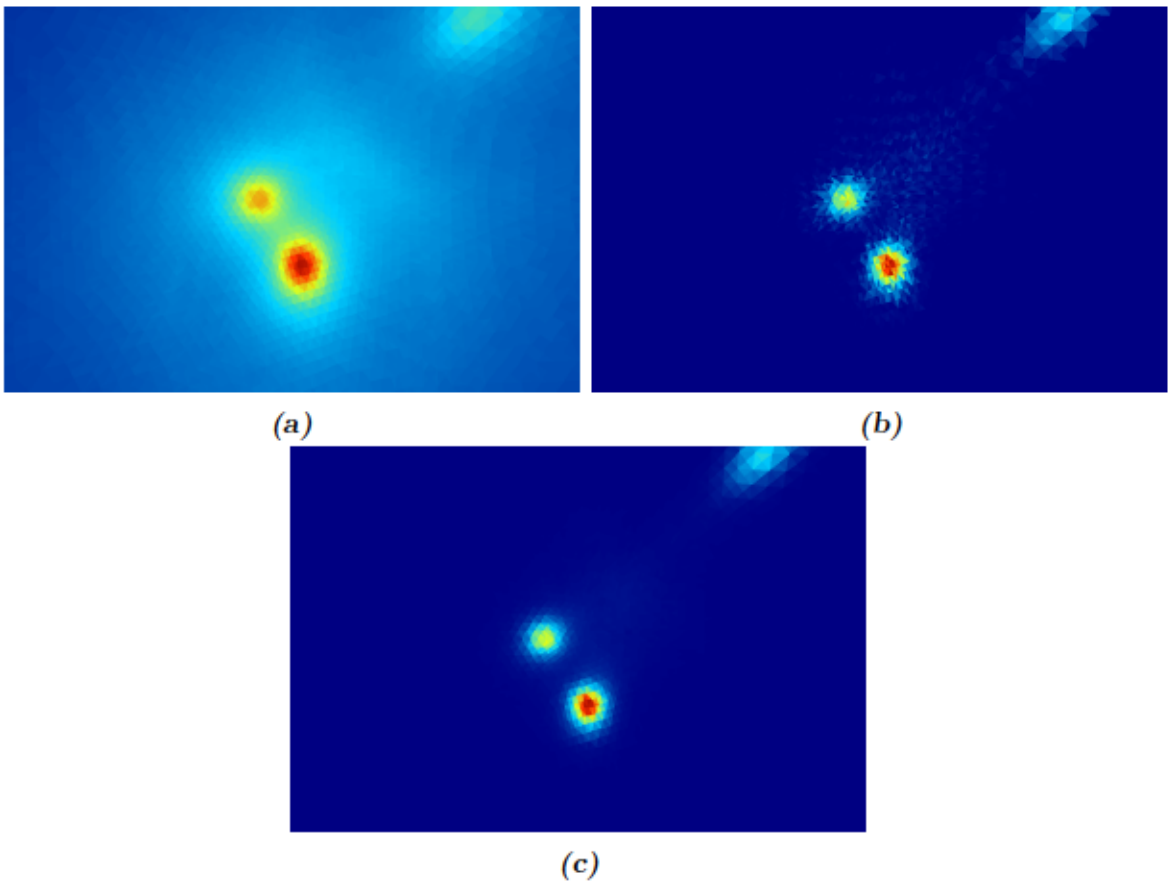

Figure 7: *Imaging of multiple sources - (a) Back Projection (b) SOE (c) LMMLEM. Leftmost source is half the intensity of the centre-most source. Furthest source is the same intensity as the centre-most, its reduced visual impact is entirely due to being off-centre with the corresponding lowered detector sensitivity.*

4.3 Eye rotation Tests

Allowing the user the functionality to move the window as with their head and visually inspect the entire field of view is a key feature to this imaging representation. The multi-source example from the previous section can be seen here with corresponding 45 degree rotations in Fig.8.

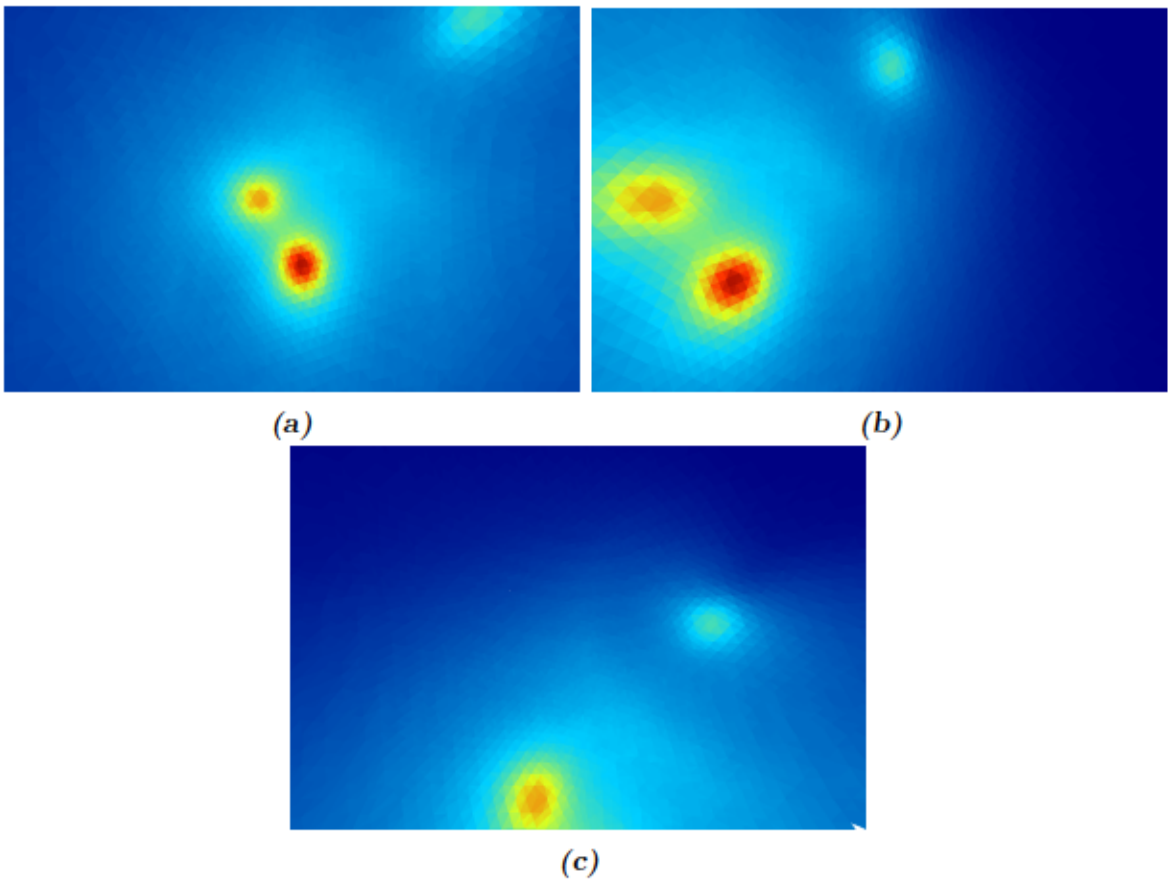

Figure 8: *The observer magic window is free to move within the geodesic tessellation - in (a) the observer is staring straight at the same three sources as the previous section, in (b) the observer tilts his head 45 degree to the right and the visualization moves as anticipated left, in (c) the observer tilts his head 45 degrees up from the centred position and the sources likewise are displaced as anticipated down.*

4.4 Real World Imaging

The final step in the Observer View is to superpose the pixelated imaging results with the view taken from the imager's camera. At the time of this report's writing the camera was still undergoing R&D. Regardless, most of the code to perform this overlay is written. Several colour and transparency schemes were devised to most clearly demonstrate the imaged data. The most pleasing to the eye is an overlay colour pattern which associates a red-blue scale over the top 50% of the imaged data, the remaining half of the image data is left transparent. A challenging picture was selected, a scene with lots of reds, oranges and yellows, typical colours used to focus attention. For the end user to discern a source it is demonstrably easier if there is high contrast within the colour palette chosen. It is not sufficient to merely demarcate activities in simple red or red/yellow, a bit of blue aids the eye enormously. At present the user does not control the palette but in future work this may be implemented.

Figure 9: *Raw image of a colorful, difficult to image bridge. Prague, capital of the once Holy Roman Empire.*

Figure 10: *Multi-source imaging back projection translucent overlay. Second source is difficult to disambiguate.*

Figure 11: *Reduced threshold and higher contrast provides much better visual source detection.*

5 Sample High Statistics Monte Carlo Visualizations of a Point Source

A ^{137}Cs point source at 10 m was simulated until it reached 200 000 golden events. In previous reports, with much lower statistics than the present study, SOE had measurable advantage in a comparative 2-D Gaussian fit of the source position relative to LMMLEM. Presently there is no source localization advantage found, within statistical uncertainty both algorithms perform equally well. However, and importantly: LMMLEM is much faster. SOE performance can improve with multiple cores and multi-threading but remains consistently slower by a factor of nearly 10.
The triangle tessellated geodesic grid does not lend itself well to quantitative analysis. Most of the projection and fitting tools work off of underlying Cartesian systems.

5.1 Back Projection

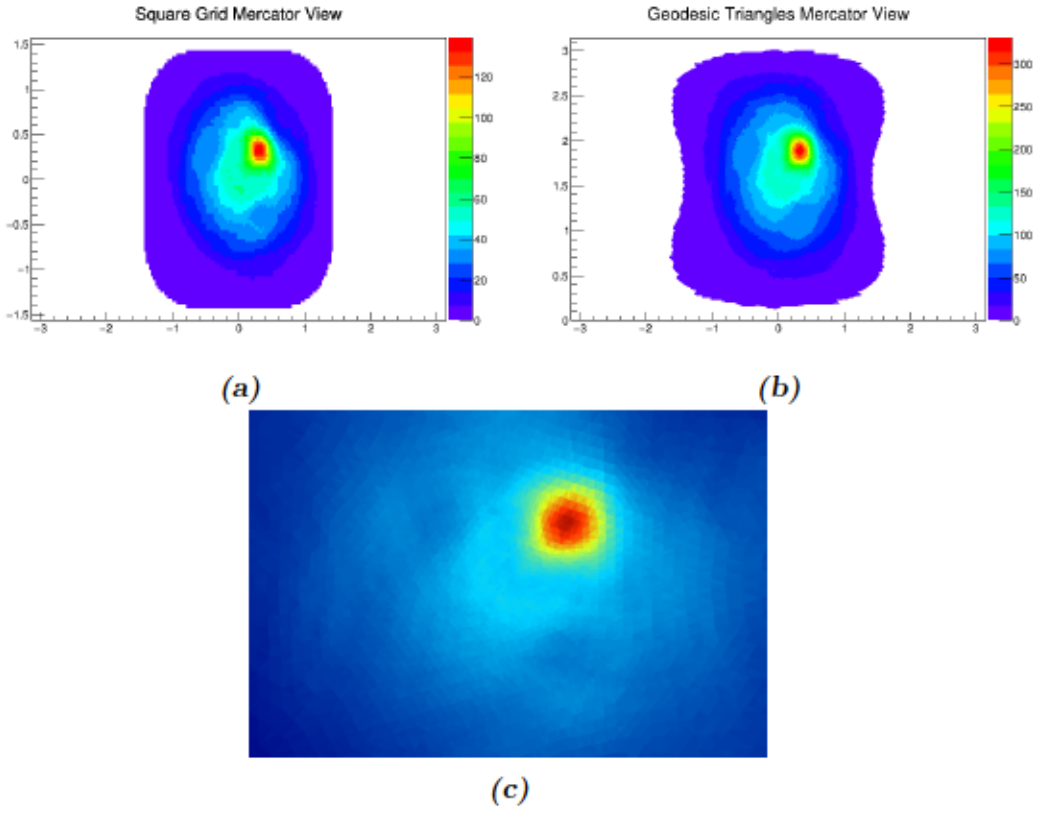

Figure 12: *Back projection, 200 000 Compton cones ^{137}Cs (a) Mercator square grid (b) Mercator geodesic triangles projection (c) Observer view. The tessellation level is set to 8 in all figures.*

5.2 LMMLEM

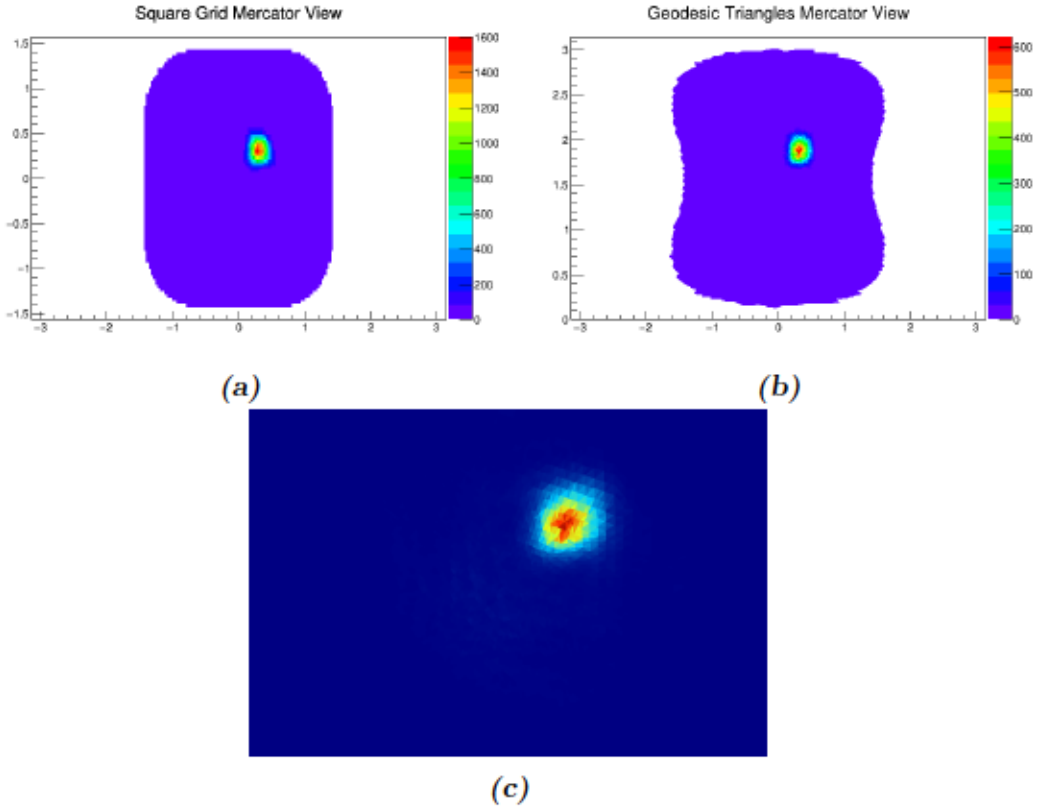

Figure 13: *LMMLEM, 200 000 Compton cones ^{137}Cs (a) Mercator square grid (b) Mercator geodesic triangles projection (c) Observer view. The tessellation level is set to 8 in all figures and the Observer window is a field of view of 112 degrees horizontally and 90 degrees vertical.*

5.3 SOE

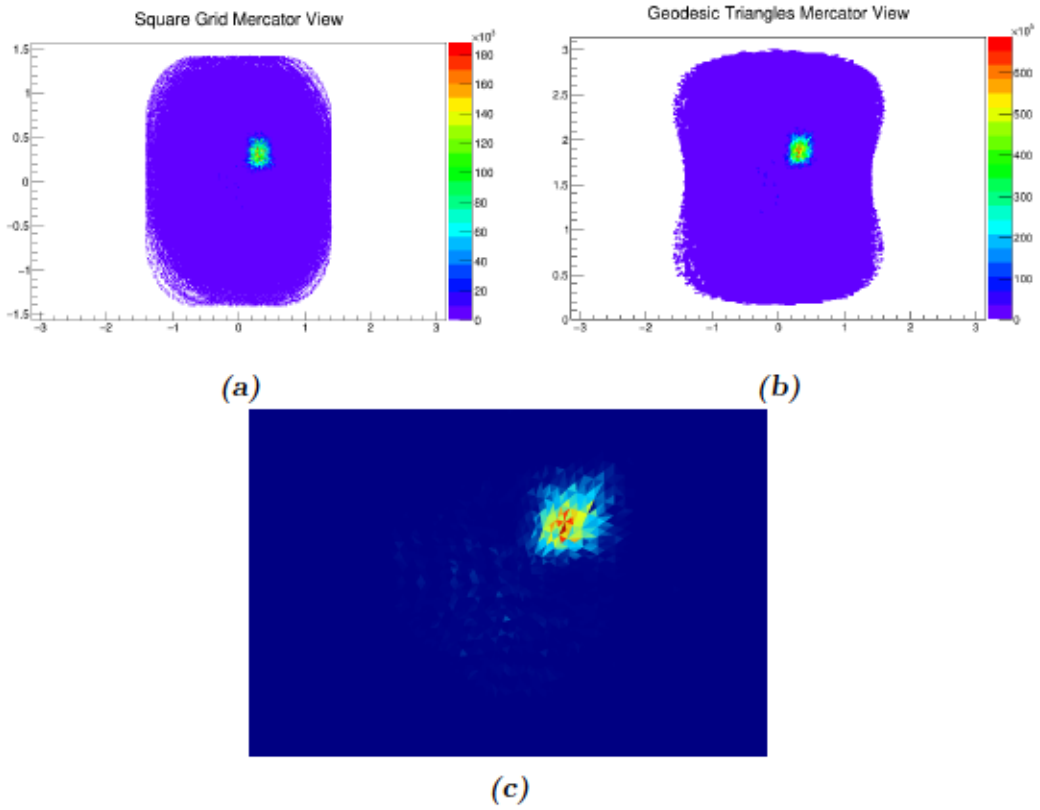

Figure 14: *SOE, 200 000 Compton cones ^{137}Cs (a) Mercator square grid (b) Mercator geodesic triangles projection (c) Observer view. The tessellation level is set to 8 in all figures and the Observer window is a field of view of 112 degrees horizontally and 90 degrees vertical.*

6 Applications and Extensions of Imaging Code

A concern amongst our collaborators was that we had merely tested the imaging code against "perfect' Monte-Carlo and real world data might reveal artifacts or problems that could not otherwise be anticipated (noise, resolution, bad data that may slip through cuts, etc...). A still additional cross check is verification of the results of a UAV survey over a very large distributed source.

6.1 Jiffy imaging

The "Jiffy' is a 2x2 Compton imager with different electronics, sensitive volume and materials than the full 3x3. Its purpose was to be a portable proof of principle design towards the final 3x3. Two short runs were imaged: a ^{137}Cs run with 12k golden events in Fig.15 and similarly a ^{22}Na run with 2k in Fig.16.

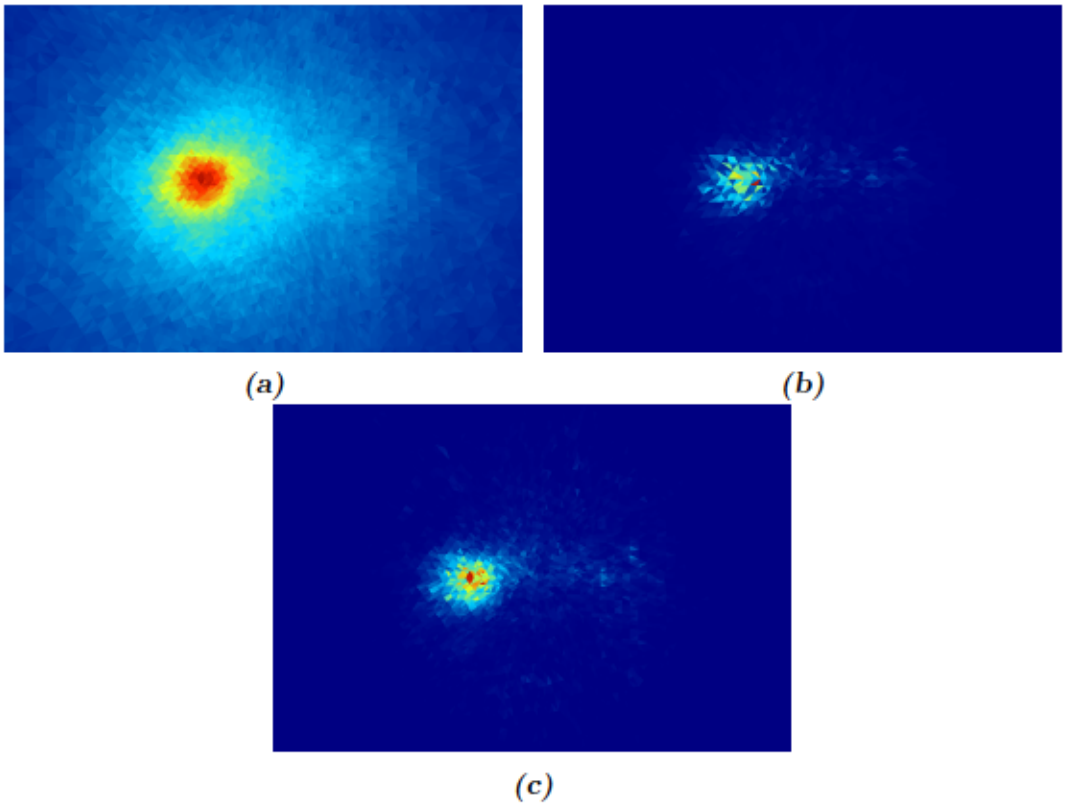

Figure 15: *Real data from Jiffy imager for ^{137}Cs (a) Back Projection (b) SOE (c) LMMLEM. The LMMLEM algorithm appears to be the winner by eye.*

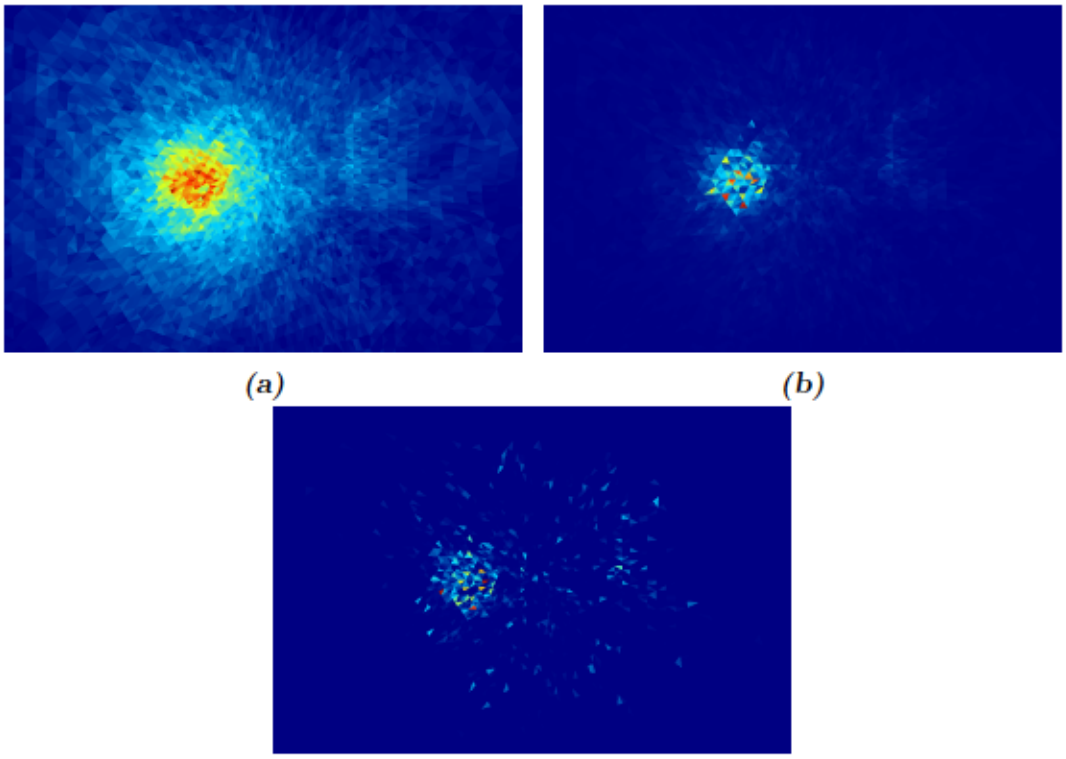

Figure 16: *Real data from Jiffy imager for* ^{22}Na *(a) Back Projection (b) SOE (c) LMMLEM. With these lower counts and this different source, factoring all the variables it appears that SOE better resolves the source. These results are a bit surprising as naively SOE should function better with larger sample size, however the main purpose of this research is to empirically test rather than speculate. The immediate conclusion from visual inspection drawn from even these limited tests: for the end user both imaging algorithms should be made available and allow their judgment in the field to prevail.*

6.2 Large and small "L" imaging

Within the RAD/NUK detection community there is little doubt as to the utility of Compton imagers, however specific applications may benefit from different approaches. One possibility when faced with a large distributed source is to mount a radiation detector on an unmanned aerial vehicle (UAV) and fly over the contaminated area. With the UAV, human life is not placed at risk and so flying quite close to the source of radiation is possible. Because all radiation detection is ultimately a trade-off vs solid angle even a simple counter might in principle suffice: simply fly it in a raster pattern close to the source with count rate alone and some careful post-processing one can in principle reveal the extent and structure of the source - no imaging required.

There was however an open question in the minds of the collaborators that perhaps instead of using a simple counter, a Compton imager mounted on the UAV might perform even better and resolve greater detail. This is not obvious, since planar Compton imagers have distinctly forward aimed sensitivity and travelling near by an extended source would have many events aimed at the sides of the imager where it is not sensitive. The percentage of "golden events" which can provide directional information is also a tiny fraction of all events (0.3%) and so the rates should also favour the simple counter in principle. However from a practical perspective if the Compton imager performed reasonably well the case could be made for simply purchasing more of the same hardware, and furthermore the imager could always been flown at a fixed high altitude to resolve a wider pan image as it is most suited, or even used exclusively in self shielding mode while flying the raster pattern.

The first source, dubbed the "large L" is composed of ^{137}Cs in two bands, one measuring 70 x 5 m and the other 60 x 10 m, each band having $5 \cdot 10^9$ Bq activity. The UAV is programmed to fly in a 150 x 150 m square grid pattern taking a single 1 second image every 10 m, flying 10 m above the surface. Instead of performing 225 simulations the simpler solution was to design a giant 225 grid of detectors and do a single simulation for 1 second. The Mercator View of each individual detector was combined with the Mercator View of the others, forming a composite image. This compositing process is a tricky projection, as cones with too large of a Compton angle cannot be easily projected, for instance a gamma calculated as arriving at 60 degrees relative to the ground normal with a 40 degree Compton angle would have portions of its ring extending beyond the 90 degree horizon. In spite of these difficulties the large L was clearly resolved in Fig.17.

The second source dubbed the "small L" is a scaled down version with bands measuring 7 x 2.5 m and 6 x 5 m, of identical activity. In the composite view one could still make out by eye the rough shape of an L, Fig.19. The best visualization of the small L is from a single detector, these fine features are smoothed out by the compositing.

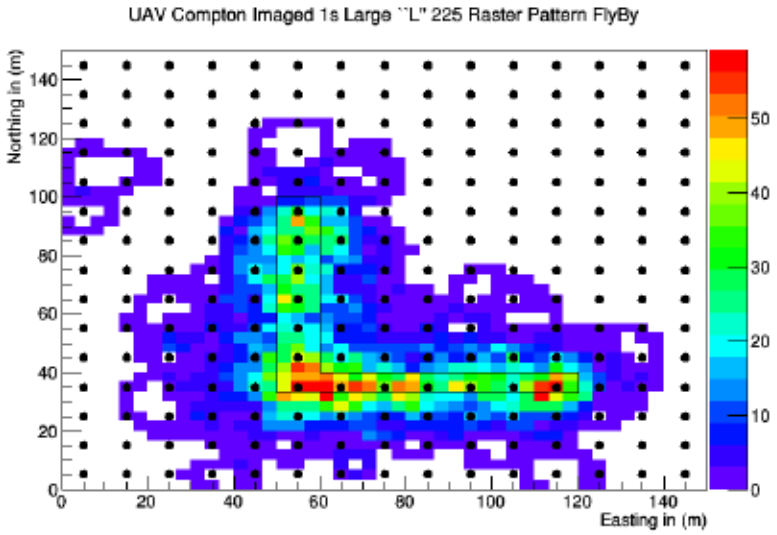

Figure 17: *The UAV is flown in a raster pattern represented by the large black dots over a large distributed "L" shaped source, seen in black outline. The Compton camera takes an image for 1 second at the location of the dots. Each resulting Mercator projection is stitched together to form a composite view, revealing the shape of the underlying activity.*

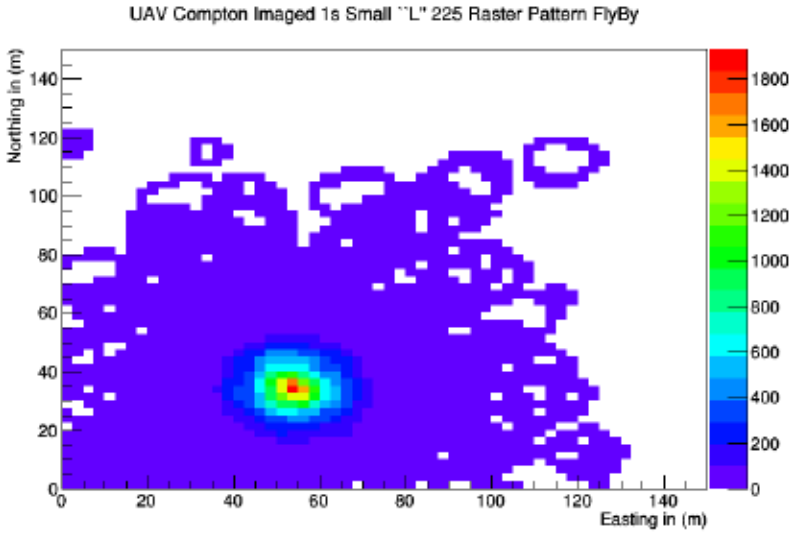

Figure 18: *Similar to Fig.17 but with a much smaller "L" source, merely 7 x 6 m. This size of distributed source is specifically at the limit of the spatial sampling and realistically once detected the individual snapshots directly above the source would be investigated and the collating multiple views from multiple angles would be foregone.*

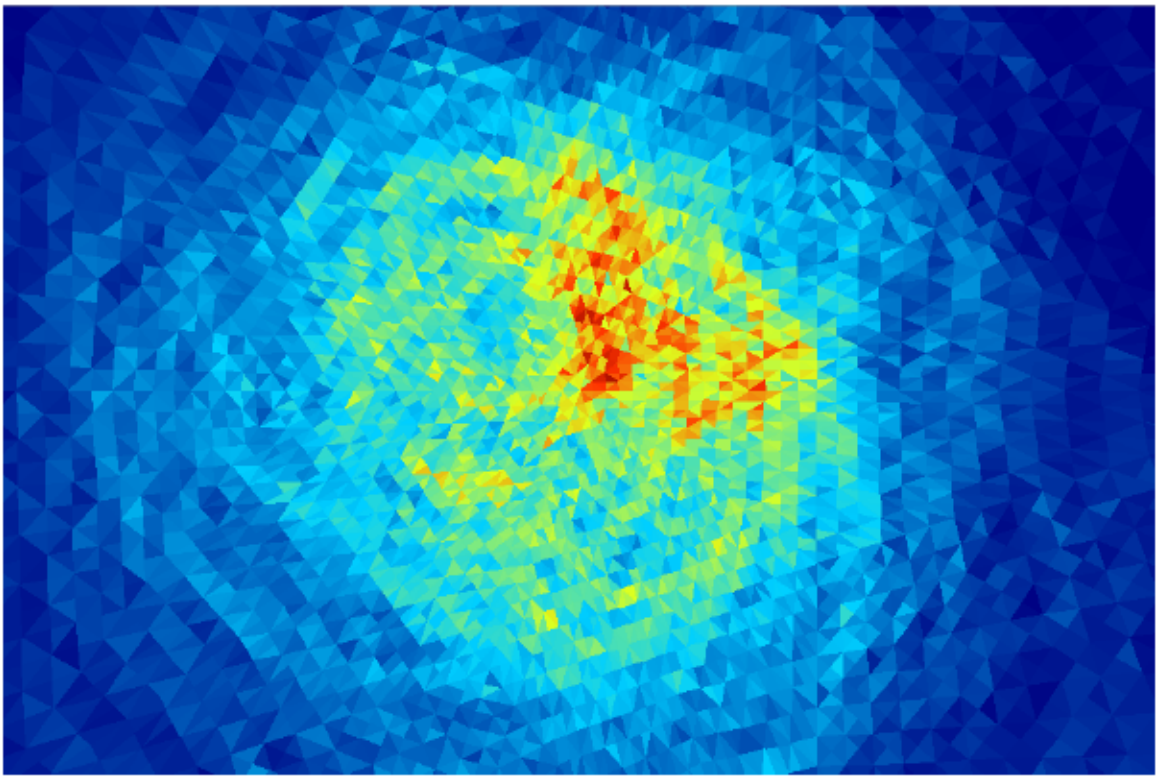

Figure 19: *The Observer View snapshot of the single position directly above the small L. The distributed source legs are clearly distinguishable.*

7 Finalized Instrument at NRC

The project as a whole was slated to come to a conclusion by end of fiscal year 2018 (March). This constrained efforts to a strict timeline, and many work-arounds were necessary to accommodate for a not-quite-complete device to ultimately successfully meet the goal.

7.1 Final physical device

The final fully functional hardware arrived at the end of December 2017, just prior to Christmas, Fig.20,22,21.

Figure 20: *The finalized imager on a cart, its camera clearly visible in front. In the background on a table, the JIFFY.*

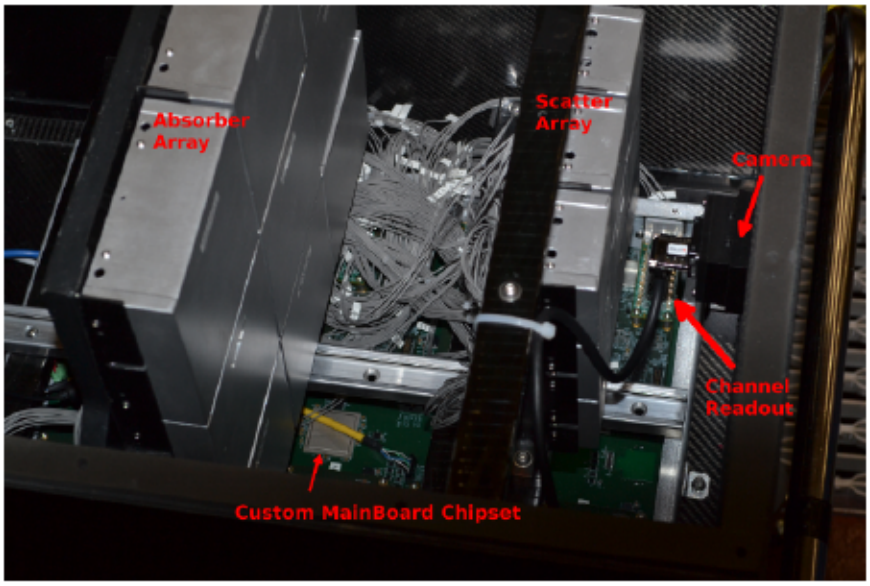

Figure 21: *Detector internals (front side). The 3x3 absorber and scatter array were mounted on rails, to preserve the option to change the focal length of the array. The mainboard sat below with its custom chipset. The SiPM were connected via the mass of cabling to channel readout daughter cards (8 in total). The camera was solidly affixed along the central symmetry axis of the array.*

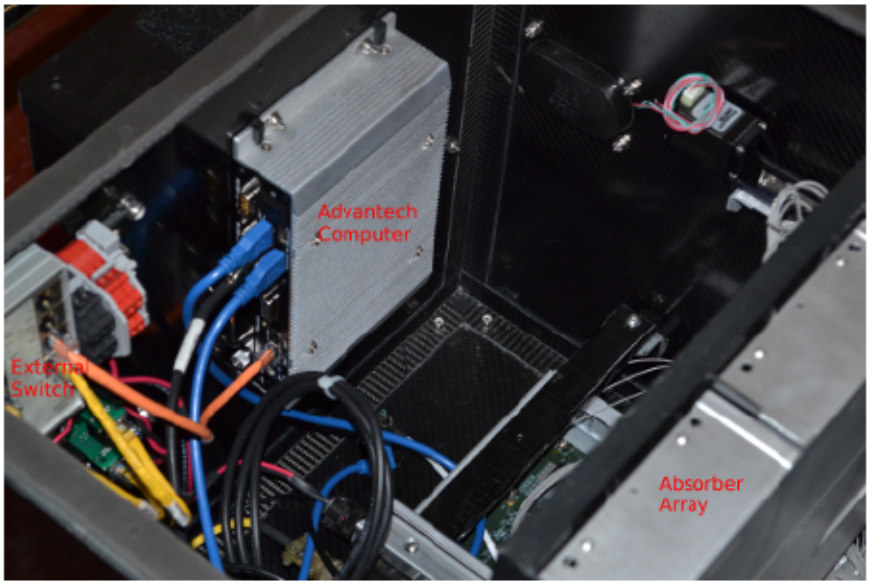

Figure 22: *Detector internals (rear side). The Advantech computer (Compton 5) communicated to the mainboard through USB. Compton 5 was in turn controlled via laptop through proprietary RAD-ASSIST software, through ethernet. A switch managed ethernet and power to the internals.*

Prior to receiving the finalized device a test-bed consisting of an incomplete set of readout boards and a 2x2 array attached to the computer "Compton 4" was available. This test bed system however did not have any attached optical camera. It was regardless essential for testing since Compton 4 was an exact duplicate of Compton 5 and much of the code could be run through the nearly-complete electronics to test for problems using synthetic and real data. An older single module array, the Jiffy, was also available and used a dissimilar code structure to run, however most importantly it had a functioning camera and could take optical images through the same lens as would be installed in the final system. Ultimately the hardware debug and fixing always took priority over the imaging. Although it introduced considerable redundancy the DRDC imaging code was installed and modified to suit all three of these systems, the final build, Compton 4 + test bed, and the Jiffy. In this way the hardware team could work in tandem with the software team with no conflicts, with software being modified first on the Jiffy and then progressed to the test bed and then onto the final build where gaps in the hardware team's schedule allowed for it.

7.2 Integration into NRC code framework

The project lead maintained full control of the final code implementation at all times. The imaging package DRDC provided at the end of the previous contract was to be integrated in stages. Firstly the stand-alone package with no modification was to be integrated by simply accessing the executable. Secondly the stand-alone package would be integrated into worker-server structure of the NRC code. Thirdly all traces of ROOT would be segregated and the worker would perform all operations in shared memory with limited to no disk writing.

The only complication with installation of the stand alone package on the various computers was build dependencies, which were readily resolved. GAIA is the NRC point source identification and imaging algorithm and it accomplished in code structure many of the goals of the DRDC imaging algorithms, as of such GAIA code was a natural starting point towards integration. A simple wrapper was written to take the text file output of a GAIA processing, convert it into a ROOT tree and feed that tree to the DRDC imaging executable. It was in this way that the first objective was met and the stand-alone functionality achieved.

The NRC code worked off of a continuously running program dubbed "Scans" which constantly probes a shared memory buffer in RAM, this was the "server". All imaging programs were designed to be continuously running as well, as "workers", and only triggered by Scans when it registered a bit flipped within memory, which itself was the result of the user hitting a GUI button. The worker GAIA code was re-written into worker DRDC code. Initially there was no pre-processing - the shared memory locations it accessed were raw data, Compton rings and noise were sifted out by the DRDC worker. It was later decided that a first stage of pre-processing benefited all workers, and would save time overall. At conclusion the only remaining data cleaning cut within the worker DRDC code is a stage to specifically exclude backscatter.

After achieving a functional version of the DRDC code in the worker/server framework the directive was to keep only the geodesic triangle imaging representation and explicitly remove all square grid and Mercator representations. The code was substantially re-written and sorted into existing NRC libraries, headers and all ROOT code was removed and replaced with C++ wherever possible. Although ROOT is free public software covered under the GPL the ultimate goal was to remove it entirely as the end product is commercial in nature. The few remaining lines of ROOT specific code in the DRDC provided imaging algorithms relate specifically to the drawing of the tesselated geodesic triangles. Other alternative, free, drawing programs were suggested such as the D3 api used in data visualization. However the constraint of maintaining everything in shared memory with no file writing whatsoever is a stiff one, and it was not clear at the time of writing if this could be achieved in D3.

Image overlay between the semi-transparent geodesic triangles imaging and the camera shot of the surroundings was originally performed by ROOT commands and accessing files. Image overlay with no disk writing was improved by using Image Magick libraries. Image Magick is the underlying code for the "Display" command in Linux, and it happens to also have a set of arcane but very powerful commands for processing image files. Transparency was also transferred from ROOT control to Image Magick and the image file from JPEG to PNG since JPEG cannot handle transparency.
The production version contained thus streamlined workers, DRDC Back projection and DRDC LMMLEM which run continuously and the functionality to keep all imaging in memory with no file writing.

7.3 Hardware limitations

The computer model selected for the imager was an Advantech ARK-1550 (Compton 4 and 5). It was an intel i5 4300U dual core 1.6 GHz processor with 8 GB DDR3 1300 MHz ram. For storage it had a single 1 TB SSD. It was slim, fanless and "ruggedized" which from all inspection meant simply that it was encased in a solid aluminum frame. It required a separate power supply, external to the enclosure.
The SOE algorithm was designed to work within a highly multi-threaded environment and tested on individual quad core server grade CPUs, and for high statistics a cluster of 140 cores. The project lead demanded the SOE worker process run in a single threaded, single core environment and produce an image within a second for several hundred rings. Despite some effort, SOE could simply never achieve the real-world in-situ imaging speed required within these constraints. It was unable to clear the 4 second mark and often ran considerably longer into the minutes range. SOE has at its base generating many more samples than simple image data manipulation and without the multi-threaded multi-core environment its performance suffered and the project lead decided to not include it in the final software package.

7.4 NRC lab testing

In all testing done in the lab the sources used were ^{137}Cs 0.5 mCu (1.8 x 10^8 Bq) and ^{22}Na 0.15 mCu (5.5 x 10^7 Bq). Empirically although these are weak sources they could readily saturate the hardware at close range. To acquire several hundred rings within a minute of running a distance of approximately 3 m was most appropriate. The hardware was also under constant tinkering and at the time of the lab tests it was impossible to acquire data for more than $\approx$ 15 minutes as circular buffers overflowed and the system crashed - this is no longer the case with the finalized instrument. Large, long, high statistics datasets were simply not possible given the accelerated timeline. Such detailed analysis will have to wait for future revisions and testing.

7.5 Adjustments for optical lens image distortion

Observer view offered the perspective of a "magic window" located at the position of the viewer's screen - and it is assumed this is a direct projection with no distortion, Fig.23. In the real device a lens was used on the camera, and the lens introduced very significant distortion and a simple projection would locate the source in the wrong location in the image, Fig.24. For the camera image and the observer view to agree the challenge was then to either: 1- distort the underlying tesselated geodesic or 2 - keep the underlying geodesic the same and distort the projection onto the observer's magic window. The latter option was ultimately successful.
After much empirical trial and error the lens was found to obey a fairly simple tangent geometric projection. In essence a line of objects equally spaced perpendicular to the central viewing axis "in angles" were distorted to produce equal spacing "linearly" on the window, Fig.25. A summer student at NRC had previously worked on the Jiffy camera system and arrived at a fairly complex angular correction factor for that specific lens. In practice however inclusion of this factor within the statistics achievable at the time of testing did not lead to any marked improvement over the simpler formulation and the simpler formulation was kept in production code, Fig.26.

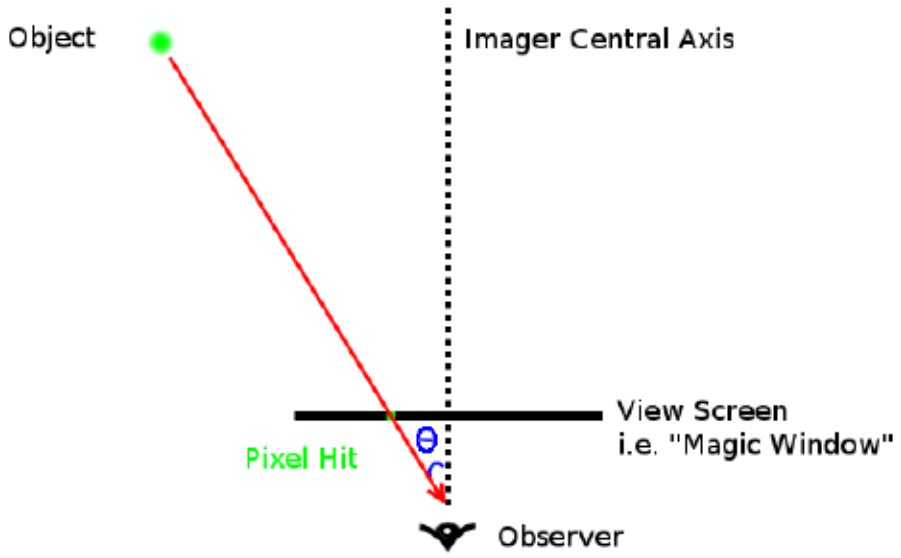

Figure 23: *The default projection assumed within "Observer View". This is a straightforward projection of a unit geodesic sphere onto the user's screen, the only knowledge required to perform this is the angle at which the observer sees through the magic window, θ, relative to the imager's central axis.*

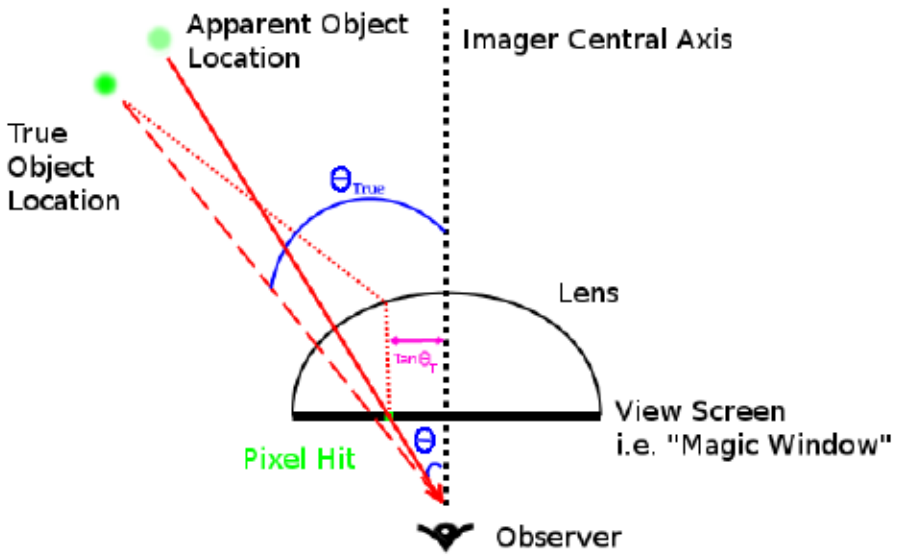

Figure 24: *In the real world application the image is captured using a camera and a lens. The lens introduces significant distortion in the optical image, however the physical angles derived from the absorber and scatter hits do not have such distortion. The problem is then to relate the apparent angle at which objects are seen in the camera projected image, θ to their true angle as seen by the imager, θ_{True}. For the specific lens used it was empirically determined a simple tangent formulation was sufficient.*

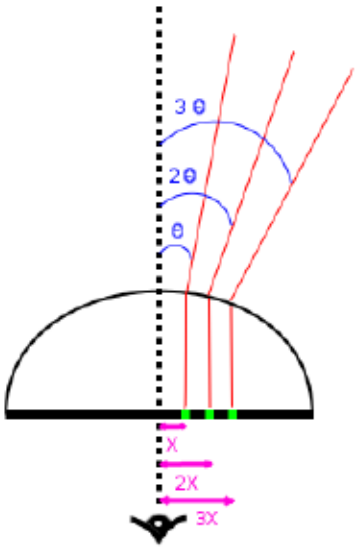

Figure 25: *The optical image was captured in 1080p format, 1920x1080 pixels. The camera was first carefully and properly aligned along the imager's central axis. An object seen at pixel X away from the central pixel corresponded to a real world angle of θ, an object seen at pixel 2X away from the central pixel corresponded to a real world angle of twice θ, and so on. Equally spaced angles were thus distorted by the lens into an equally spaced line.*

Figure 26: *Camera imaging of the NRC test hall. The large red dot represents the true source position (top). The yellow and black striped tape on the ground is in fact a straight line in the real world, it appears warped into a curve as a result of the lens. With the angular correction applied (bottom) back projection Observer View overlays properly with the off-axis source in the display.*

7.6 Field testing of the completed system

Field testing of the imager was performed at RCMP-TPOF in March 2018. The same NRC sources as used in lab testing were hidden within a variegated urban environment testing ground. The imager mounted in a van was slowly rolled through the test area to try and locate and identify the sources. A similar exercise was performed at the port of Montreal with shipping containers. The imager was found to perform well in both instances, only experiencing some difficulty with moving sources. The detailed results of these tests cannot be reported here.
Here follow images of the RAD-ASSIST software using the fully functional integrated DRDC imaging package to visualize a source at NRC after its return from the field.

Figure 27: *End-user imaging of a ^{137}Cs source at NRC part 1. This image is a screen shot capture of the RAD-ASSIST program which runs on a laptop connected to the Compton imager. On the left is a continuously updating "waterfall" plot of the energy spectrum: every 1 second the energy spectrum is read out and continuously incrementing from below in a coloured band. This allows for the user to potentially identify changes in the detected radiation based on energy alone. In this instance the source has remained in its fixed location and the spectrum has been accumulating for 10 minutes. The sum energy spectrum, the projection of the waterfall plot is displayed in the bottom left corner and the Cs line is clearly visible. The user has yet to engage imaging and merely knows from the energy spectrum and alarms that something is present but is unaware of the source location.*

Figure 28: *End-user imaging of a ^{137}Cs source at NRC part 2. The user has selected a band in the waterfall plot corresponding to the energy peak of his interest. The imaging algorithm is thus activated and in less than 1 second the geodesic LMMLEM is overlayed upon the camera output identifying the most probably location of the radioactivity successfully.*

7.7 Potential improvements

This project was a private/public partnership and as of such the private company must turn a profit from the manufacture and sale of these devices. This project has also been a lengthy endeavour, spanning many years and with many people's input that are no longer directly affiliated with it. The conclusion is certainly the device works, and works well, however upon final review some of the decisions made could have been better and here follows a list of suggestions a potential future upgrade should consider.

As identified earlier the weakest component of the system is the computer. Mini-ITX form factor off-the-shelf systems designed for a rugged small footprint are no longer merely the realm of computer enthusiasts. 32 GB DDR4 (not DDR3, DDR4) ram is standard fare and 64 GB can be readily achieved. Clock speeds of 2400 MHz is also standard, once again compared to 1300. APUs have also come a long way today, these chips combine onboard graphics and quad-core CPUs all on the same die, retail Ryzen 2200g at the time of writing this is merely 130 $ and 4x as fast as the Advantec. Although the SSD is of decent quality and considerable size, what this system necessitates is speed, and gains of 3-4x could be achieved by using modern NVME (any higher end MLC such as the 960 pro for instance). The only real advantage to the ARK-1550 is that it is passively cooled but this may not be a real advantage in the end. More air flow within the enclosure would likely homogenize temperature within and thus negates individual crystal temperature drift. Fans are also quite reliable and in the worst case: easy and cheap to replace. If maintaining the power-supply external to the enclosure is a real concern Pico-PSU motherboard power adapters are a simple solution for applications under 200 Watts (which the current system is well below). In this regard the computer is perhaps the weakest link in the system, certainly sufficient, but barely so. With a more powerful off-the-shelf computer advanced algorithms such as SOE could definitely be used in a future upgrade. Considerable time and effort was spent optimizing algorithms for speed to try and reach real world thresholds based on a slow computer, whereas the option of simply using a faster computer could have been taken. The upside is that the current work will not be lost, should a fast computer be used with the current extremely fast algorithms it would be possible to envision other applications, such as responsive tracking of moving sources.

The power supply chosen was also a no-name industrial supply which was overly warm and noisy, once again much superior off-the-shelf parts exist for limited cost increase considering the final price of the device.

In the author's opinion the fibre glass enclosure is ugly, moreover the footprint relative to the internals could be reduced, and this was clearly the private company's purview. This is a bit of a shame with such a space age device, a little more effort in the cosmetic design department could streamline the enclosure with no functional sacrifice.

8 Summary and Conclusions

The DRDC effort in the Compton imaging project led by NRC has produced a variety of powerful imaging algorithms and a novel means of displaying the imager information.

- Three imaging algorithms, Back Projection, LMMLEM and SOE were developed and highly optimized for speed.
- Several end-user imaging representations were developed in particular a novel recursive tessellated geodesic Observer View.
- The algorithms were tested against real and simulated data successfully.
- All algorithms perform well and are not confused by multiple sources.
- The code package was produced in a stand-alone format and sufficiently general to be used for any Compton imager.
- Distributed sources were simulated alongside a UAV application of a simplified imager, and the algorithms once again performed well.
- The DRDC code was modified and merged within existing NRC code.
- Additional modifications to fit the finalized hardware were successful.
- The commercial production version instrument now exists and has passed several field tests.
- The project as a whole has achieved its goals, on time.

In closing several options exist for improvement should they be desired by the Canadian Armed Forces. A final imaging code was investigated: a simulation based likelihood function. Such a simulation based algorithm would in theory produce the most realistic source reconstruction and eliminate many of the assumptions within the other algorithms particularly how the angular detector response is assumed uniform - but also address finer points such as how the Compton cones are assumed to be infinitesimal thickness rings rather than fuzzy probability bands. The requisite extensive simulations to build the likelihood function were deemed premature, as hardware was still being assembled in the final months of the project. Effort was focused on producing functional final codes that would work irrespective of the details. In the future, the simulation based likelihood function could be resurrected.
It is the opinion of the author that the weakest point of the entire system has been identified as the internal computer, and an upgrade of this part is straightforward.

References

[1] Saull, P. et al. (2012), First demonstration of a Compton gamma imager based on silicon photomultipliers, *Nuclear Instruments and Methods in Physics Research A*, 679, 89–96.

[2] Sinclair, L. et al. (2014), Silicon Photomultiplier-Based Compton Telescope for Safety and Security (SCoTSS), *Proc IEEE Trans. Nucl. Sci.*, 61, 2745 – 2752.

[3] Phillips, G. (1995), Gamma-ray imaging with Compton cameras, *Nuclear Instruments and Methods in Physics Research B*, 99, 674–677.

[4] Sinclair, L., Saul, P., et al. (2014), Silicon Photomultiplier Based Compton Telescope for Safety and Security, *IEEE Transactions on Nuclear Science*, 61, 2745.

[5] Lam, J. (2015), SCoTSS Geant4 Design and Simulation, (DRDC-RDDC-2015-C113) Defence Research and Development Canada – Ottawa Research Centre.

[6] Ueno, R. (2016), Development of the GEANT4 Simulation for the Compton Gamma-Ray Camera, (DRDC-RDDC-2016-C138) Defence Research and Development Canada – Ottawa Research Centre.

[7] Brun, R. and Rademakers, F., ROOT - An Object Oriented Data Analysis Framework, *Nucl. Inst. & Meth. in Phys. Res. A*, 389(1997), 81–86. See also http://root.cern.ch/.

[8] Doxygen (online), Dimitri van Heesch, http://www.doxygen.org (Access Date: August 2017).

[9] Todd, R., Nightingale, J., and Everett, D. (1974), A proposed gamma camera, *Nature*, 251, 132–134.

[10] Barrett, H. H., White, T., and Parra, L. C., List-mode likelihood, *J. Opt. Soc. Am. A*, 14(1997), 2914–2923.

[11] Wilderman, S. et al., List-mode maximum likelihood reconstruction of Compton scatter camera images in nuclear medicine, *Proc IEEE Nuclear Science Symposium*, 3(1998), 1716 – 1720.

[12] Hamel, M., Polack, J., et al. (2017), Localization and spectral isolation of special nuclear material using stochastic image reconstruction, *Nuclear Instruments and Methods in Physics Research A*, 841, 24–33.

[13] Andreyev, A., Sitek, A., and Celler, A. (2011), Fast image reconstruction for Compton camera using stochastic origin ensemble approach, *Med. Phys.*, 38, 429–438.

[14] Hastings, W. (1970), Monte Carlo sampling methods using Markov chains and their applications, *Biometrika*, 57, 97–109.

[15] Drouin, P.-L. (2016), Markov Chain Monte Carlo and Stochastic Origin Ensembles Methods, (DRDC-RDDC-2016-R124) Defence Research and Development Canada – Ottawa Research Centre.

DOCUMENT CONTROL DATA

*Security markings for the title, authors, abstract and keywords must be entered when the document is sensitive

1. ORIGINATOR (Name and address of the organization preparing the document. A DRDC Centre sponsoring a contractor's report, or tasking agency, is entered in Section 8.)

Zernam
1701 Woodward Dr, Suite 100
Ottawa, ON K2C 0R4
Canada

2a. SECURITY MARKING (Overall security marking of the document including special supplemental markings if applicable.)

CAN UNCLASSIFIED

2b. CONTROLLED GOODS

NON-CONTROLLED GOODS
DMC A

3. TITLE (The document title and sub-title as indicated on the title page.)

Development of Advanced Imaging Algorithms and Representations for Compton Gamma-Ray Cameras

4. AUTHORS (last name, followed by initials – ranks, titles, etc., not to be used)

Ouellet, C. V.

5. DATE OF PUBLICATION (Month and year of publication of document.)	6a. NO. OF PAGES (Total pages, including Annexes, excluding DCD, covering and verso pages.)	6b. NO. OF REFS (Total references cited.)
April 2018	46	15

7. DOCUMENT CATEGORY (e.g., Scientific Report, Contract Report, Scientific Letter.)

Contract Report

8. SPONSORING CENTRE (The name and address of the department project office or laboratory sponsoring the research and development.)

DRDC – Ottawa Research Centre
Defence Research and Development Canada
3701 Carling Avenue
Ottawa, Ontario K1A 0Z4
Canada

9a. PROJECT OR GRANT NO. (If appropriate, the applicable research and development project or grant number under which the document was written. Please specify whether project or grant.)	9b. CONTRACT NO. (If appropriate, the applicable number under which the document was written.)
	W7714-4501560211

10a. DRDC PUBLICATION NUMBER (The official document number by which the document is identified by the originating activity. This number must be unique to this document.)	10b. OTHER DOCUMENT NO(s). (Any other numbers which may be assigned this document either by the originator or by the sponsor.)
DRDC-RDDC-2018-C074	

11a. FUTURE DISTRIBUTION WITHIN CANADA (Approval for further dissemination of the document. Security classification must also be considered.)

Public release

11b. FUTURE DISTRIBUTION OUTSIDE CANADA (Approval for further dissemination of the document. Security classification must also be considered.)

12. KEYWORDS, DESCRIPTORS or IDENTIFIERS (Use semi-colon as a delimiter.)

3D imaging; Compton imager; radiation detection

13. ABSTRACT/RESUME (When available in the document, the French version of the abstract must be included here.)

DRDC has produced a toolkit of imaging algorithms which are suitable for any segmented Compton gamma ray imager. The algorithms incorporate a completely novel, three dimensional tessellated geodesic mesh representation for the data. The geodesic representation is fully recursive to include arbitrary resolution and furthermore resolves projection artifacts of other common imaging systems. As part of the partnership between DRDC, NRC and Radiation Solutions Inc., a fully functional rugged Compton imager has been successfully manufactured for the Canadian Armed Forces. DRDC imaging algorithms have been integrated into the imager software and provide reliable, fast options for radioactive threat detection.

RDDC a produit une boîte à outils d'algorithmes d'imagerie qui conviennent à tout imageur à rayons gamma Compton segmenté. Les algorithmes incorporent une représentation en treillis géodésique tridimensionnelle complètement nouvelle pour les données. La reprèsentation géodésique est entièrement récursive pour inclure une résolution arbitraire et résout en outre les artefacts de projection d'autres systèmes d'imagerie courants. Dans le cadre du partenariat entre RDDC, le CNRC et Radiation Solutions Inc., un imageur Compton robuste et entièrement fonctionnel a été fabriqué avec succès pour les Forces Armées Canadiennes. Les algorithmes d'imagerie de RDDC ont été intégrés dans le logiciel de l'imageur et o˙rent des options fiables et rapides pour la détection des menaces radioactives.